Porphine Homocoupling on Au(111)

K. Seufert,[Δ,1] F. McBride,[Δ,2] S. Jaekel,[1] B. Wit,[2] S. Haq,[2] A. Steiner,[1]
P. Poli,[2] M. Persson,[*,2] R. Raval,[*,2] L. Grill[*1]

[1)] *Dept. of Physical Chemistry, University of Graz, Austria*

[2)] *Surface Science Research Centre, Dept. of Chemistry, University of Liverpool, U.K.*

[Δ] Equal Contributions

[*] Corresponding authors:

mats.persson@liverpool.ac.uk (MP; theory), phone: +44 151 794 3518

r.raval@liverpool.ac.uk (RR; experimental), phone: +44 151 794 6981

leonhard.grill@uni-graz.at (LG; experimental), phone: +43 316 380 5410

ABSTRACT: The covalent coupling of porphine molecules on Au(111) is studied by scanning probe microscopy experiments and density functional theory. At sufficient temperatures, dehydrogenative C-C coupling of the unfunctionalised molecules occurs directly on the surface. Characteristic dimer structures between individual porphine molecules are observed and assigned to various binding motifs that are distinguished by specific intermolecular connections. Different preparations show that the relative abundance of these motifs depends on the temperature of the gold sample during deposition, explained by calculated free energies and kinetic aspects that are relevant during the linking process. Observations on the gold terraces are completed by studying polymerization at step edges, giving insight into their role during the covalent linking process.

INTRODUCTION

During the past decades, covalently bound nanostructures have attracted significant research interest[1-4] with porphyrin being a frequently used building block.[5-9] Nanostructures built from porphyrin derived molecules have shown promise as chromophores,[5, 10-13] for molecular electronics,[5, 14, 15] gas sensing,[16] charge storage,[17] and for nonlinear optics.[18, 19] While small oligomers and especially dimers have been deposited successfully on surfaces for analysis,[20-22] problems occur for larger species and the use of traditional wet chemistry methods for synthesis and subsequent deposition on surfaces is restricted by limitations either in solubility for deposition from solution or in thermal stability for sublimation from the solid state.

One way is to synthesize the structures directly on the surface from monomeric building blocks.[1, 3, 6, 23] To achieve covalent bonding the monomers can either be synthesized with linking groups - such as halogens,[6, 24, 25] alkynes,[26, 27] mesityl[7, 28] or amines[29] for coupling reactions – or by directly fusing the macrocycles of neighboring porphyrins by forming C-C bonds between them (i.e. *meso*-*meso*, β-β, or β-*meso*; Figure 1). Because the presence and type of linking groups influence the physical properties of the oligomers,[8, 18, 20, 30-34] the specific bonding scheme is of particular importance. Direct dehydrogenative C-C coupling has been achieved by heating monomers under UHV conditions on noble metal surfaces: free-base porphyrins (2H-P) on Ag(111)[35, 36] and diphenyl-porphyrins (DPP) on Cu(111).[37] This coupling method has the advantage of maintaining conjugation throughout the oligomer and not leaving byproducts to contaminate the surface.[7, 38] In both cases, the reaction products are dominated by oligomers, in which the individual porphyrin units are connected through six-membered carbon rings – two rings for (β-β) + (*meso*-*meso*) + (β-β) bonded connections or one ring for (β-*meso*) + (*meso*-β) bonded connections. As the binding influences the physical properties of the oligomer,[20, 33, 34] producing different motifs is valuable for tuning the product properties. Herein, we show that dehydrogenative C-C coupling of unfunctionalized porphine occurs directly on the Au(111) surface and that the occurrence of various binding motifs between porphine

molecules at different temperatures can be related to the free energies of the various species and kinetic aspects that are relevant during the linking process.

EXPERIMENTAL

Porphine molecules (2H-P, Figure 1) were deposited onto a clean Au(111) surface (prepared by standard surface science techniques) through sublimation from a Knudsen cell at a temperature of about 210 °C (rates of about 0.2 ± 0.1 ML/min). Polymerization of the molecules is induced thermally by heating the sample, either during or after molecule deposition (in the latter case the sample is kept at room temperature during deposition). Imaging was done by scanning tunnelling microscopy (STM) in constant-current mode with the sample kept mostly at around 5 K during imaging (otherwise the imaging temperature is indicated).

RESULTS AND DISCUSSION

(i) Molecular Adsorption. When 2H-P is adsorbed on a sample kept at room temperature during deposition, no molecular islands are formed (Figure 2a), although the temperature is sufficient to allow molecular diffusion of porphyrin derivatives on Au(111).[39] Instead of assembling into close-packed structures, the molecules adsorb as isolated entities oriented with their diagonal axis along one of the substrate's high symmetry directions. At very low coverages of about 0.18 ML, the distribution of molecules is not random, but follows the corrugation of the characteristic herringbone reconstruction of the Au(111) surface (Figure 2a). Specifically, the molecules prefer adsorption on fcc over hcp areas (see Figure S1), a known behavior for molecules on Au(111).[40-43] At the same time, the molecules maintain a spacing towards each other (instead of close-packing), suggesting a repulsive interaction between molecules, similar to that observed for the same molecules on the Ag(111) surface.[44]

When depositing more molecules, the intermolecular spacing decreases (Figure 2b-e) and the preferred adsorption on fcc areas are lost. The molecules now also adsorb on hcp areas or on the ridges of the herringbone reconstruction, covering the entire surface equally and leaving the herringbone reconstruction unchanged (visible as bright lines from bottom left to top right in Figure 2d). However, even at a coverage of one full monolayer, no close-packing of the molecules takes place, as evident from the fact that neighboring molecules can have different orientations (Figure 2d). The molecules are, therefore, still at a distance that ensures sufficient degrees of freedom to change their orientation – in contrast to close-packed layers.[45]

If the monolayer coverage is exceeded (note that this transition defines the coverage of exactly one monolayer), a second layer grows in a densely packed phase with equal orientation for all molecules (Figure 2e). Therefore, the molecule-molecule interaction must be different for molecules adsorbed on metal as compared to those overlaying other molecules, in agreement with a substrate-mediated repulsion mechanism as found for 2H-P on Ag(111).[44]

Fourier transformation of the STM data (Figure 2f-j) shows spots at coverages above 0.4 ML which is typical for a repulsive interaction where molecules try to maximise the intermolecular distance and are finally forced into a regular pattern.[44] The complete monolayer (Figure 2i) reveals various periodicities that can be assigned either to the herringbone reconstruction (stripe around the origin) or to the molecules (spots at larger inverse lengths). We determine a value of 10.1 ± 0.3 Å as the dominating intermolecular distance for the first layer (Figure 2i), while the average distance measured over many molecules in real space images is 11.6 ± 0.3 Å. This can be understood by a close inspection of Figure 1d. While most molecules tend to be in close proximity to their next neighbors (which gives rise to the dominating periodicity of 10.1 Å), occasionally a larger distance can be observed – leading to the distinction of dominating and average distances.

In the second layer the 2H-P no longer shows four-fold symmetry but instead one corner of the molecule appears brighter whilst the opposite corner is no longer visible (Figure 2j). We assume

a tilt of the porphines with respect to the surface, leading to different distances between molecules depending on the direction in the highly ordered hexagonal assembly. The short distance – along the tilted molecules – is 9.5 ± 0.3 Å while the long distance is 10.2 ± 0.3 Å, close to the dominating distance in the monolayer.

(ii) Porphine Dimerization at Terraces. After characterization of the adsorbed molecules, the formation of oligomers was induced by depositing 2H-P molecules onto a heated Au(111) surface. The sample was held at different (constant) temperatures during each individual preparation (indicated in Figure 3). Imaging the surface afterwards shows that the surface coverage decreases with increasing temperature although the molecular flux and deposition time are always the same. This suggests increased desorption probability of the molecular state as the surface temperature is increased. At 450 °C sample temperature only few molecules remain on the surface (Figure 3e).

In addition to the monomers, various new molecules appear (indicated by circles in Figure 3), which were never observed when the sample was kept at room temperature during deposition (Figure 2). Although the dominant species on the surfaces are always monomers (see grey ring in Figure 4e), different types of molecular oligomers are also present. We focus here on the dimers since they are the initial product during polymerization and represent the majority of oligomers (100% of the reaction products are dimers for deposition at a sample temperature of 250 °C, 90% at 300 °C, 60% at 350 °C, 38% at 400 °C and 50% at 450 °C).

Nature of the Dimer Motifs. The characteristic appearances and orientations of the porphine molecules in a dimer or oligomer and their relative positions with respect to each other enable us to identify distinct binding motifs (Figure 4) with the help of DFT calculations (calculated gas phase structures are shown at the bottom of Figure 4a-d): (A) single C-C bond between β positions of both molecules; (B) (β-β), (β-*meso*) motif with two C-C bonds in a five-membered ring configuration; (C) (β-*meso*), (*meso*-β) motif with two C-C bonds in a six-membered ring; (D) (β-β), (*meso*-*meso*), (β-β) motif with three C-C bonds in two six-membered rings (an overview is given in Figure 5). Note that

the possible assignment of dimer A to a double C-C bond between adjacent β-β positions on each molecule is ruled out from our DFT calculations by its much larger formation energy than the single C-C bond, due to the creation of a highly strained four-membered carbon ring (see Figure 5b and gas phase data in Figure S5). The existence of a number of products, including the creation of both five-membered and six-membered carbon rings, already hints that energetics is not the only factor determining the reaction products since otherwise only one reaction product should be observed.

An important observation is that the relative abundance of the experimentally observed motifs strongly depends on the sample temperature. As shown in Figure 4e, motifs A and B are dominant while C and D can be found in small numbers. At 250 °C, which was the lowest successful reaction temperature in our experiments, only binding motifs A and B were present. With increasing temperature, two main trends are observed in the distribution of reaction products: (1) Starting at 350 °C, the ratio of motifs A and B tips in favor of motif B, after previously favoring motif A and (2) motifs C and D start to appear at 300 °C. In addition, the molecular density drops with increasing temperature, also evident in the STM images (Figure 3), which can be understood from thermal desorption of the monomers (oligomer desorption can be ruled out, due to their higher adsorption energies; see Supporting Information).

As motif B includes a β-β bond, which is also found in motif A, the first trend (1) can be explained through a conversion of existing motif A connections forming another (β-*meso*) bond to close a five-membered ring after expulsion of H_2. For this purpose, one of the molecules has to rotate out of its preferred orientation. Selective desorption of species A can be ruled out as the reason for the trend since the surface density does not drop sufficiently between 300 °C and 350 °C where the flip in population occurs.

In terms of total reaction yield there is a clear increase in the fraction of reaction products (from 2% to 22%) when increasing the substrate temperature from 250 °C to 350 °C. And while there is a decrease in the surface density of reacted molecules (surface density × fraction of reacted

molecules; Figure 4e) from 0.076 to 0.071 mol/nm^2 when going from 350 °C to 400 °C, this decrease (6%) is much less pronounced than the decrease in molecular density overall (~25%). Hence, the increase in the fraction of reacted molecules with temperature is not only caused by on-surface reactions, but also by monomer desorption (smaller adsorption energy than for dimers).

Energetics and Selectivity in Product Formation. A central question is what causes the selectivity in the formation of the different dimers, mainly motifs A and B. We have studied whether the relative orientation of neighboring close-packed monomers within a close-packed monolayer plays a role. However, the result (Figure S2) does even at low temperatures not show any clear correlation, suggesting that the distribution of binding motifs is not caused by a pre-orientation of the monomers but is primarily driven by reaction kinetics. Note that the molecular orientation during the reaction can differ from the orientation at imaging conditions (5 K). This is reflected in the reorientation of one porphine in motif B that is no longer aligned with the substrate's high symmetry directions.

In order to gain more insight into the on-surface dimerization reactions and their pathways, we have carried out density functional theory (DFT) calculations of the on-surface reaction thermodynamics. The calculations show that the porphine monomers and dimers are adsorbed at distances typical for physisorption on the surface. Furthermore, for physisorption of such rather flat molecules the adsorption energy should scale roughly with the number of atoms within the molecule (0.07 eV/atom).[46] The calculated reaction (potential) energies $\Delta_r E$ for the various dimers formed from two monomers by the reaction (see Supporting Information),

$$2\mathrm{P}* \rightarrow \mathrm{P}(-n\mathrm{H})_2 * + n\mathrm{H}_2 \quad (1)$$

are shown in Figure 5b. Here P* and P(-*n*H)$_2$* is the adsorbed monomer and dimer, respectively, H_2 is the hydrogen molecule in the gas-phase, and n = 1, 2 and 3 gives the number of C-C couplings between the two monomers in the dimer. Note that the difference between the formation energy on the surface and in the gas-phase is simply given by twice the adsorption energy of the monomer minus

the adsorption energy of the dimer (see Supporting Information). The adsorption energy is defined here as the energy gain upon adsorption. The trend of the calculated $\Delta_r E$ in Figure 5b closely follows the calculations for $\Delta_r E$ in the gas phase as expected for physisorption (see gas phase data in Figure S5).

The rather large positive values for $\Delta_r E$ suggests that the on-surface dimerization reactions should not be feasible. However, the feasibility is determined by the Gibbs free energy, $\Delta_r G$, of formation and not $\Delta_r E$. The free energy includes energy and entropy contributions from the translation, rotational and vibrational motion of the molecules, which become very important at elevated temperature. In particular, the entropy contribution to $\Delta_r G$ from the translational motion of the hydrogen gas under the ultrahigh vacuum conditions of the experiments is very important.[28] At a typical background pressures of about 10^{-10} mbar and 350 °C, this contribution is about -2.4 eV per hydrogen molecule (see Table S1). In addition, we have estimated the energy and the entropy contribution to $\Delta_r G$ from the translational and rotational motion of the adsorbed monomers and dimers (see Supporting Information). For example, this contribution is about 1.4 eV for all dimers at 350 °C (see Table S1), primarily due to the decrease in entropy for the translational and rotational motions when forming dimers from two monomers. The resulting reaction (Gibbs) free energies, $\Delta_r G$, are shown in Figure 5c at a temperature of 350 °C. Note that the relative values of $\Delta_r G$ with the same number of C-C couplings are not influenced by the energy and entropy contributions from the monomers and the dimers to $\Delta_r G$ and are the same as for $\Delta_r E$. In contrast, the relative values $\Delta_r G$ of dimers with a different number of C-C couplings are influenced strongly by the entropic contribution from the hydrogen gas to $\Delta_r G$ and are very different from the corresponding relative values of $\Delta_r E$.

The large contribution from the entropy of the hydrogen gas that is produced in the reaction in the vacuum chamber now makes the on-surface dimerization reaction feasible at elevated temperatures (Figure 5c). In particular, multiple C-C bonding is strongly favored by this contribution, because the entropy gain of the H_2 molecule exceeds the potential energy to form C-C bonds and the

entropic loss of the dimers with respect to the monomers. Thus, from these calculations of the reaction thermodynamics one would expect that at elevated temperatures all monomers react and form exclusively triple-bonded dimers (and oligomers). However, this expectation is in disagreement with experiments. Thus, under prevailing experimental conditions the on-surface dimerization reaction is governed by kinetics and energy barriers. The calculations of these barriers, which would include pathways where the H atoms end up in the gas phase, either directly or via the surface, are currently too computationally expensive for us to carry out. This task could be mitigated by using the Bell-Evans-Polanyi principle.[47, 48] Despite the importance of kinetics and reaction energy barriers, as discussed below, the calculated reaction free energies provide useful information about possible reaction pathways and can rationalize the observed dimerization reactions.

Since each molecule offers two types of bonding sites (denoted by *meso* and β, see Figure 1), there are three inequivalent options for how two monomers can link by a single C-C coupling: (β-β), (*meso*-*meso*) and (β-*meso*) (which is equivalent to (*meso*-β)) motifs; see Figure 5). In the case of β-β bond formation there are two possible arrangements of the two monomers with respect to each other: $(\beta\text{-}\beta)_1$ and $(\beta\text{-}\beta)_2$ (Figure 5a). All these dimer motifs are twisted and non-planar due to steric hindrance between the two monomers. Their adsorption energies are therefore substantially less than twice the adsorption energy of the monomers, which makes their formation (potential) energies to be about 0.5-1.8 eV larger than in the gas phase, with the $(\beta\text{-}\beta)_1$ being the energetically most favored one. The formation energies for $(\beta\text{-}\beta)_2$, (β-*meso*) and (*meso*-*meso*) are 0.25, 1.24 and 1.55 eV, respectively, higher in energy than $(\beta\text{-}\beta)_1$. In the gas phase, $(\beta\text{-}\beta)_1$ and $(\beta\text{-}\beta)_2$ are nearly degenerate in energy (see Figure S5) but this degeneracy is lifted on the surface by the larger adsorption energy of the more planar $(\beta\text{-}\beta)_1$ than for the less planar $(\beta\text{-}\beta)_2$ (as visible in Figure 5a). This energy splitting explains why, despite their very small difference in energy of about 0.01 eV in the gas phase, only $(\beta\text{-}\beta)_1$ is present after the formation of a single intermolecular C-C bond at the surface while $(\beta\text{-}\beta)_2$ is absent.

As a consequence, the preference of $(\beta\text{-}\beta)_1$ after the first step also explains why (β-β)(β-*meso*) (motif B in Figure 4) dominates after heating at higher temperatures and the formation of a second C-C bond. If we rule out a rotation of one porphine in the dimer around the (β-β)-bond, only the (β-β)(β-*meso*) dimer can be formed from $(\beta\text{-}\beta)_1$ by a second C-C bond formation whilst keeping the initial β-β bond intact (Figure 4b). At a sample temperature of 450 °C this leads to a very high selectivity for motif B (96%) and a yield of 26%. The other options for dimers connected by two C-C bonds would be the $(\beta\text{-}meso)^2$, (β-β)(*meso-meso*), $(\beta\text{-}\beta)^2{}_1$and $(\beta\text{-}\beta)^2{}_2$ dimers. Here the $(\beta\text{-}\beta)^2{}_2$ is formed by two adjacent β-β bonds whereas the $(\beta\text{-}\beta)^2{}_1$ is formed by two non-adjacent β-β bonds. The $(\beta\text{-}meso)^2$ dimer (motif C) is the energetically most favored double-bonded dimer due to the formation of a six-membered C ring but this dimer can only be formed from a (β-*meso*) dimer, which is energetically disfavored by about 0.55 eV compared to $(\beta\text{-}\beta)_1$ and is accordingly not observed on the surface after the first bond formation. The formation of a highly strained four-membered C-ring in the $(\beta\text{-}\beta)^2{}_2$ dimer strongly disfavors this dimer energetically by about 3 eV compared to the (β-β)(β-*meso*) and $(\beta\text{-}meso)^2$ dimers. Despite the steric constraints for the H atoms in the β and the *meso* positions of the (β-β)(*meso-meso*) and the $(\beta\text{-}\beta)^2{}_1$ dimers, respectively, these dimers are energetically about as favorable on the surface as the adsorbed (β-β)(β-*meso*) dimer. However, these two dimers can only be formed by a single C-C coupling from the energetically disfavored $(\beta\text{-}\beta)_2$ dimer. From these considerations the evolution of (β-β)(β-*meso*) from $(\beta\text{-}\beta)_1$ – once the activation energy is available – appears sensible. Hence, the on-surface reaction seems to be controlled by kinetics as the second bond formation occurs in existing single-bonded dimers, which are preferentially the motif $(\beta\text{-}\beta)_1$. Accordingly, the final products must have this structure as intermediate species.

A similar reasoning explains why triple-bonded dimers $(\beta\text{-}\beta)^2$(*meso-meso*) (motif D) are very rare and appear only at rather high temperatures, because they cannot be formed by a single C-C coupling from the abundant double-bonded dimer (β-β)(*meso-meso*). Instead, they can only be formed by a single second C-C coupling from the (β-β)(*meso-meso*) and $(\beta\text{-}\beta)^2{}_1$ dimers which should be rare

on the surface, due to the strong suppression of their precursor $(\beta\text{-}\beta)_2$ compared to $(\beta\text{-}\beta)_1$ on the surface.

(iii) Porphine Oligomerization at Steps. The dehydrogenative homocoupling of porphine molecules can extend towards long oligomers and polymeric networks using an alternative experimental protocol in which 2H-P was deposited onto a Au(111) surface at room temperature and the sample subsequently annealed to induce reaction. The sample is then cooled back to room temperature for imaging. This protocol enables molecular mobility at the surface, with STM images showing that this initially leads to decoration of steps with the molecular species (Fig S3.1). Subsequent heating to higher temperatures leads to polymeric products, formed from hundreds of individual porphine molecules that extend over long distances across the surface (Figure S3.2). The reacted products appear first at the step edges with product abundance reflecting the balance between sufficient thermal energy to access the reaction energy barriers versus competitive desorption of the monomer. Thus, after a 300 °C anneal (Figure 6a) only a small fraction of the adsorbed molecules reacts, generating short oligomers at the step edges. The presence of unreacted, diffusing molecules at the step and terrace sites is revealed as streaks in the room temperature STM images. Increasing the anneal temperature to 340 °C (Figure 6b) results in increasing oligomer length along the step edge with short branches beginning to emerge from the steps and propagating onto the terraces. By 360 °C (Figure 6c), there is significant extension of the polymeric product across the terraces, manifest as long branched chains and networks with the majority connected to a step edge. These polymeric structures appear to be random in their growth and do not favor any particular crystallographic direction for propagating across the terrace. When the temperature is increased directly to 380 °C, desorption of the monomer competes with the reaction, resulting in a lower product yield, with the oligomers largely confined to the step-edges. Finally, very large polymeric networks can be created by slight variance of the synthesis protocol whereby deposition at room temperature is followed by

successive annealing cycles to progressively higher temperatures, with re-cooling to room temperature before each heating step (Figure S3).

The relative abundance of the different types of porphine-porphine connections within the oligomers formed at step sites across the 300 to 380 °C temperature range are also shown in Figure 6. Overall, there is a significant increase in the incidence of motifs C and D at the step sites, representing the creation of the most energetically favored (β-*meso*)^2 the (β-β)^2(*meso*-*meso*) couplings shown in Figure 5. The effect of steps upon the distribution of bonding motifs is even more pronounced when the porphine is deposited onto a hot crystal. Figure 7a-b compares statistics at step and terrace sites when 2H-P is deposited on the Au(111) surface at 300 °C, showing that the relative proportions of motifs C and D are increased by approximately two and six, respectively, at step sites as compared to terraces (Figure S4). Here, D is the major bonding motif with high proportions of the next two most thermodynamically stable products B and C and only a small quantity of motif A.

It, therefore, appears that the presence of step edges makes a significant contribution (quantified in Figure 7a-b) to the creation of the most energetically stable motifs C and D, despite the relatively high temperatures that are used to induce polymerization, which indicates that homocoupling takes indeed preferentially place at the step edges. Note that preferential adsorption of motifs C and D at step edges cannot be excluded from the experiments as origin of the observed differences of product distributions on terraces vs. step edges. However, our DFT data suggest that the generation of motifs C and D on terraces is unlikely (as discussed below).

We would not anticipate that motifs D and C would occur via a concerted multiple C-H bond breaking and C-C bond making process at step edges since this would require extremely high activation energies. However, an important factor here is that spatial confinement and alignment of neighboring porphine molecules at step sites would make the formation of motif D (straight edges) and motif C (kinked edges) more likely as sketched in Figure 7c. The stabilization of other single C-C bonding motifs beside A is crucial in opening up the increased formation of motifs C and D. For

example, the singly bonded $(\beta\text{-}\beta)_2$ species is a suitable candidate to act as precursor to motif D, but the $(\beta\text{-}\beta)_2$ motif is less planar than motif A and is 0.25 eV higher in energy when adsorbed on a flat terrace. However, the presence of a surface step may reduce the energy penalty for the formation of such a non-planar precursor motif, opening up a pathway to motif D. Similarly, the (β-*meso*) precursor to motif C is markedly higher in energy (1.24 eV) at a terrace but, again, may be accessible at a step site. Motif C could alternatively be formed via β-β bond breaking in motif B, again facilitated by the presence of a step, allowing a second β-*meso* bond to be formed, thus exchanging the strained five membered ring for the energetically more favorable six membered ring of motif C. Finally, DFT calculations could verify the suggested preference of the adsorption of various motifs on the step edges, but these calculations are very challenging due to the large number of atoms needed to represent these system and are well beyond the scope of this work.

The catalytic activity of undercoordinated metal atoms at step edges of metallic surfaces is well known.[49, 50] Step edges may alter reaction products in a number of ways: providing confined environments that pre-align porphines prior to reaction, offer additional degrees of freedom (tilt angle and bend) for the molecule that are not accessible when simply adsorbed to the flat terrace, enhance the stability of non-planar precursors, or, alter the energy barriers to interconversion of bonding motifs towards the more energetically stable product. Specifically on the Au(111) surface, several previous studies of on-surface reactions have highlighted the important role of temperature, step edges and elbows on the resulting products.[51-54] For instance, we note that studies of cyano-substituted porphine derivatives on Au(111) have found molecular arrangements stabilised at step edges that are not seen on terraces.[55] We, therefore, suggest that the reason we produce the thermodynamically most stable product (motif D) efficiently only at the step edge is pre-alignment of molecules at step edges, forcing them into a co-linear arrangement (Figure 7c), with the step topography also enabling the non-planar $(\beta\text{-}\beta)_2$ precursor to become energetically accessible.

CONCLUSIONS

Adsorption of porphine on Au(111) in the submonolayer regime results in separated molecules, instead of close-packed islands, probably due to substrate-mediated repulsion since the second monolayer behaves differently. Upon sample heating molecular dimerization occurs resulting in various products, with the precise coupling motif dependent on the temperature. Analysing the abundance of these dimers in combination with calculations reveals that the reactions are governed by energy barriers and kinetics. In contrast to the gas phase, the twisting angle of two molecules linked by one C-C bond in a dimer becomes important on the surface as it results in a higher adsorption energy for the more planar species. Consequently, certain reaction pathways are preferred on the terraces, even after formation of a second bond between the monomers. Step edges facilitate the growth of porphine oligomers with an altered distribution of bonding motifs that is probably influenced by that the spatial molecular confinement at steps.

Acknowledgements

S. J. and L. G. thank the European Marie Curie Initial Training Network (ITN) for financial support through the ACRITAS project. R.R. thanks EPSRC (EP/J019364/1, EP/K039687/1, EP/N51004X/1) for financial support that partly supported this work. P.P. and M.P. acknowledge computer time allocated on ARCHER and THOMAS through or membership of the Materials Chemistry Consortium (EPSRC grant no. EP/L000202**,** EP/R029431,EP/P020194) and on Chadwick at the University of Liverpool.

Supporting Information Available: Adsorption with respect to the Au(111) herringbone reconstruction; molecular orientation; porphine at steps and large polymer networks; bonding motif distribution after deposition at 300 °C; estimating the rates for oligomer desorption; computational

details; calculated reaction energies for dimerisation in the gas phase; free-energy calculations. This material is available free of charge via the Internet at http://pubs.acs.org.

REFERENCES

1. Gourdon, A. On-surface covalent coupling in ultrahigh vacuum. *Angew. Chem. Int. Ed.* **2008,** *47*, 6950-6953.
2. Colson, J. W.; Dichtel, W. R. Rationally synthesized two-dimensional polymers. *Nat Chem* **2013,** *5* (6), 453-465.
3. Klappenberger, F. Two-dimensional functional molecular nanoarchitectures - Complementary investigations with scanning tunneling microscopy and X-ray spectroscopy. *Prog. Surf. Sci.* **2014,** *89*, 1-55.
4. Held, P. A.; Fuchs, H.; Studer, A. Covalent-bond formation via on-surface chemistry. *Chem. Eur. J.* **2017,** *23*, 5874-5892.
5. Tsuda, A.; Osuka, A. Fully conjugated porphyrin tapes with electronic absorption bands that reach into infrared. *Science* **2001,** *293*, 79-82.
6. Grill, L.; Dyer, M.; Lafferentz, L.; Persson, M.; Peters, M. V.; Hecht, S. Nano-architectures by covalent assembly of molecular building blocks. *Nat. Nanotech.* **2007,** *2*, 687-691.
7. Veld, M. I.; Iavicoli, P.; Haq, S.; Amabilino, D. B.; Raval, R. Unique intermolecular reaction of simple porphyrins at a metal surface gives covalent nanostructures. *Chem. Commun.* **2008**, 1536-1538.
8. Tanaka, T.; Osuka, A. Conjugated porphyrin arrays: synthesis, properties and applications for functional materials. *Chem. Soc. Rev.* **2015,** *44*, 943-969.
9. Haq, S.; Hanke, F.; Sharp, J.; Persson, M.; Amabilino, D. B.; Raval, R. Versatile bottom-up construction of diverse macromolecules on a surface observed by scanning tunneling microscopy. *ACS Nano* **2014,** *8*, 8856-8870.
10. Lin, V. S.; DiMagno, S. G.; Therien, M. J. Highly conjugated, acetylenyl bridged porphyrins: new models for light-harvesting antenna systems. *Science* **1994,** *264*, 1105-1111.
11. Elemans, J. A. A. W.; Hameren, R. v.; Nolte, R. J. M.; Rowan, A. E. Molecular materials by self-assembly of porphyrins, phthalocyanines, and perylenes. *Adv. Mater.* **2006,** *18*, 1251-1266.
12. Yella, A.; Lee, H.-W.; Tsao, H. N.; Yi, C.; Chandiran, A. K.; Nazeeruddin, M. K.; Diau, E. W.-G.; Yeh, C.-Y.; Zakeeruddin, S. M.; Grätzel, M. Porphyrin-sensitized solar cells with Cobalt(II/III)-based redox electrolyte exceed 12 percent efficiency. *Science* **2011,** *334*, 629-634.
13. Li, L.-L.; Diau, E. W.-G. Porphyrin-sensitized solar cells. *Chem. Soc. Rev.* **2013,** *42*, 291-304.
14. Kuang, G.; Chen, S.-Z.; Wang, W.; Lin, T.; Chen, K.; Shang, Y.; Liu, P. N.; Lin, N. Resonant charge transport in conjugated molecular wires beyond 10 nm range. *J. Am. Chem. Soc.* **2016,** *138*, 11140-11143.
15. Peeks, M. D.; Tait, C. E.; Neuhaus, P.; Fischer, G. M.; Hoffmann, M.; Haver, R.; Cnossen, A.; Harmer, J. R.; Timmel, C. R.; Anderson, H. L. Electronic delocalization in the radical cations of porphyrin oligomer molecular wires. *J. Am. Chem. Soc.* **2017,** *139*, 10461-10471.
16. Nguyen, T. Q.; Escano, M. C. S.; Shimoji, N.; Nakanshi, H.; Kasai, H. Adsorption of diatomic molecules on iron tape-porphyrin: A comparative study. *Phys. Rev. B* **2008,** *77*, 195307.
17. Lindsey, J. S.; Bocian, D. F. Molecules for charge-based information storage. *Acc. Chem. Res.* **2011,** *44*, 638-650.
18. Cho, H. S.; Jeong, D. H.; Cho, S.; Kim, D.; Matsuzaki, Y.; Tanaka, K.; Tsuda, A.; Osuka, A. Photophysical properties of porphyrin tapes. *J. Am. Chem. Soc.* **2002,** *124*, 14642-14654.

19. Kim, D. Y.; Ahn, T. K.; Kwon, J. H.; Kim, D.; Ikeue, T.; Aratani, N.; Osuka, A.; Shigeiwa, M.; Maeda, S. Large two-photon absorption (TPA) cross-section of directly linked fused diporphyrins. *J. Phys. Chem. A* **2005,** *109*, 2996-2999.
20. Takagi, A.; Yanagawa, Y.; Tsuda, A.; Aratani, N.; Matsumoto, T.; Osuka, A.; Kawai, T. STM images of individual porphyrin hexamers; *meso-meso* singly linked orthogonal hexamer and *meso-meso*, β−β, β−β triply-linked planar hexamer on Cu(100) surface. *Chem. Commun.* **2003**, 2986-2987.
21. Zimmerman, J. D.; Diev, V. V.; Hanson, K.; Lunt, R. R.; Yu, E. K.; Thompson, M. E.; Forrest, S. R. Porphyrin-tape/C_{60} organic photodetectors with 6.5% external quantum efficiency in the near infrared. *Adv. Mater.* **2010,** *22*, 2780-2783.
22. Krasnikov, S. A.; Sergeeva, N. N.; Sergeeva, Y. N.; Senge, M. O.; Cafolla, A. A. Self-assembled rows of Ni porphyrin dimers on the Ag(111) surface. *Phys. Chem. Chem. Phys* **2010,** *12*, 6666-6671.
23. Lackinger, M.; Heckl, W. M. A STM perspective on covalent intermolecular coupling reactions on surfaces. *J. Phys. D: Appl. Phys.* **2011,** *44*, 464011.
24. Lafferentz, L.; Eberhardt, V.; Dri, C.; Africh, C.; Comelli, G.; Esch, F.; Hecht, S.; Grill, L. Controlling on-surface polymerization by hierarchical and substrate-directed growth. *Nat. Chem.* **2012,** *4*, 215-220.
25. Lin, T.; Shang, X. S.; Adisoejoso, J.; Liu, P. N.; Lin, N. Steering on-surface polymerization with metal-directed template. *J. Am. Chem. Soc.* **2013,** *135*, 3576-3582.
26. Zhang, Y.-Q.; Kepcija, N.; Kleinschrodt, M.; Diller, K.; Fischer, S.; Papageorgiou, A. C.; Allegretti, F.; Björk, J.; Klyatskaya, S.; Klappenberger, F.; Ruben, M.; Barth, J. V. Homo-coupling of terminal alkynes on a noble metal surface. *Nat. Comm.* **2012,** *3*, 1286.
27. Gao, H.-Y.; Wagner, H.; Zhong, D.; Franke, J.-H.; Studer, A.; Fuchs, H. Glaser coupling at metal surfaces. *Angew. Chem. Int. Ed.* **2013,** *52*, 4024-4028.
28. Floris, A.; Haq, S.; Veld, M. I.; Amabilino, D. B.; Raval, R.; Kantorovich, L. Driving forces for covalent assembly of porphyrins by selective C−H bond activation and intermolecular coupling on a copper surface. *J. Am. Chem. Soc.* **2016,** *138*, 5837-5847.
29. Chen, C.; Joshi, T.; Li, H.; Chavez, A. D.; Pedramarazi, Z.; Liu, P.-N.; Li, H.; Dichtel, W. R.; Bredas, J.-L.; Crommie, M. F. Local electronic structure of a single-layer porphyrin-containing covalent organic framework. *ACS Nano* **2018,** *12*, 385-391.
30. Wojaczynski, J.; Latos-Grazynski, L. Poly- and oligometalloporphyrins associated through coordination. *Coord. Chem. Rev.* **2000,** *204*, 113-171.
31. Mohnani, S.; Bonifazi, D. Supramolecular architectures of porphyrins on surfaces: The structural evolution from 1D to 2D to 3D to devices. *Coord. Chem. Rev.* **2010,** *254*, 2342-2362.
32. Nakamura, Y.; Aratani, N.; Shinokubo, H.; Takagi, A.; Kawai, T.; Matsumoto, T.; Yoon, Z. S.; Kim, D. Y.; Ahn, T. K.; Kim, D.; Muranaka, A.; Kobayashi, N.; Osuka, A. A directly fused tetrameric porpyrin sheet and its anomalous electronic properties that arise from the planar cyclooctatetraene core. *J. Am. Chem. Soc.* **2006,** *128*, 4119-4127.
33. Richert, S.; Limburg, B.; Anderson, H. L.; Timmel, C. R. On the influence of the bridge on triplet state delocalization in linear porphyrin oligomers. *J. Am. Chem. Soc.* **2017,** *139*, 12003-12008.
34. Gao, G.; Kang, H. S. Engineering of the electronic structures of metal-porphyrin tapes and metal-hexaphyrin tapes: A first-principles study. *Chem. Phys* **2010,** *369*, 66-70.
35. Wiengarten, A.; Seufert, K.; Auwärter, W.; Ecija, D.; Diller, K.; Allegretti, F.; Bischoff, F.; Fischer, S.; Duncan, D. A.; Papageorgiou, A. C.; Klappenberger, F.; Acres, R. G.; Ngo, T. H.; Barth, J. V. Surface-assisted dehydrogenative homocoupling of porphine molecules. *J. Am. Chem. Soc.* **2014,** *136* (9346-9354).

36. Bischoff, F.; He, Y.; Riss, A.; Seufert, K.; Auwärter, W.; Barth, J. V. Exploration of interfacial porphine coupling schemes and hybrid systems by bond-resolved scanning probe microscopy. *Ang. Chem. Int. Ed.* **2018,** *57*, 16030-16035.
37. Xiang, F.; Gemeinhardt, A.; Schneider, M. A. Competition between dehydrogenative organometallic bonding and covalent coupling of an unfunctionalized porphyrin on Cu(111). *ACS Nano* **2018,** *12*, 1203-1210.
38. Haq, S.; Hanke, F.; Dyer, M. S.; Persson, M.; Iavicoli, P.; Amabilino, D. B.; Raval, R. Clean coupling of unfunctionalized porphyrins at surfaces to give highly oriented organometallic oligomers. *J. Am. Chem. Soc.* **2011,** *133*, 12031-12039.
39. Mielke, J.; Hanke, F.; Peters, M. V.; Hecht, S.; Persson, M.; Grill, L. Adatoms underneath single porphyrin molecules on Au(111). *J. Am. Chem. Soc.* **2015,** *137*, 1844-1849.
40. Vladimirova, M.; Stengel, M.; Vita, A. D.; Baldereschi, A.; Böhringer, M.; Morgenstern, K.; Berndt, R.; Schneider, W.-D. Supramolecular self-assembly and selective step decoration on the Au(111) surface. *Europhys. Lett.* **2001,** *56*, 254-260.
41. Lafferentz, L.; Ample, F.; Yu, H.; Hecht, S.; Joachim, C.; Grill, L. Conductance of a single conjugated polymer as a continuous function of its length. *Science* **2009,** *323*, 1193-1197.
42. Cirera, B.; Trukhina, O.; Björk, J.; Bottari, G.; Rodriguez-Fernandez, J.; Martin-Jimenez, A.; Islyaikin, M. K.; Otero, R.; Gallego, J. M.; Miranda, R.; Torres, T.; Ecija, D. Long-range orientational self-assembly, spatially controlled deprotonation, and off-centered metalation of an expanded porphyrin. *J. Am. Chem. Soc.* **2017,** *139*, 14129-14136.
43. Hanke, F.; Björk, J. Structure and local reactivity of the Au(111) surface reconstruction. *Phys. Rev. B* **2013,** *87*, 235422.
44. Bischoff, F.; Seufert, K.; Auwärter, W.; Joshi, S.; Vijayaraghavan, S.; Ecija, D.; Diller, K.; Papageorgiou, A. C.; Fischer, S.; Allegretti, F.; Duncan, D. A.; Klappenberger, F.; Blobner, F.; Han, R.; Barth, J. V. How surface bonding and repulsive interactions cause phase transformations: Ordering of a prototype macrocyclic compound on Ag(111). *ACS Nano* **2013,** *7*, 3139-3149.
45. Gross, L.; Moresco, F.; Ruffieux, P.; Gourdon, A.; Joachim, C.; Rieder, K.-H. Tailoring molecular self-organization by chemical synthesis: Hexaphenylbenzene, hexa-peri-hexabenzocoronene, and derivatives on Cu(111). *Phys. Rev. B* **2005,** *71*, 165428.
46. Björk, J.; Hanke, F.; Palma, C.-A.; Samori, P.; Cecchini, M.; Persson, M. Adsorption of aromatic and anti-aromatic systems on graphene through π-π stacking. *J. Phys. Chem. Lett.* **2010,** *1*, 3407-3412.
47. Bell, R. P. The theory of reactions involving proton transfers. *Proc. R. Soc. London A* **1937,** *154* (882), 414-429.
48. Evans, M. G.; Polanyi, M. Further considerations on the thermodynamics of chemical equilibria and reaction rates. *Trans. Faraday Soc.* **1936,** *32*, 1333-1360.
49. Zambelli, T.; Wintterlin, J.; Trost, J.; Ertl, G. Identification of the "active sites" of a surface-catalyzed reaction. *Science* **1996,** *273*, 1688-1690.
50. Saywell, A.; Schwarz, J.; Hecht, S.; Grill, L. Polymerization on stepped surfaces: Alignment of polymers and identification of catalytic sites. *Angew. Chem. Int. Ed.* **2012,** *51*, 5096-5100.
51. Sk, R.; Arra, S.; Dhara, B.; Miller, J. S.; Kabir, M.; Deshpande, A. Effect of cyano substitution on the step-edge adsorption of copper phthalocyanine on Au(111) *J. Phys. Chem. C* **2018,** *11848-11854*.
52. Peyrot, D.; Silly, M. G.; Silly, F. Effect of cyano substitution on the step-edge adsorption of copper phthalocyanine on Au(111) *J. Phys. Chem. C* **2017,** *121*, 26815-26821.
53. Peyrot, D.; Silly, F. On-surface synthesis of two-dimensional covalent organic structures versus halogen-bonded self-assembly: Competing formation of organic nanoarchitectures. *ACS Nano* **2016,** *10*, 5490-5498.

54. Arado, O. D.; Mönig, H.; Wagner, H.; Franke, J.-H.; Langewisch, G.; Held, P. A.; Studer, A.; Fuchs, H. On-surface azide-alkyne cycloaddition on Au(111). *ACS Nano* **2013,** *7*, 8509-8515.
55. Pham, T. A.; Song, F.; Alberti, M. N.; Nguyen, M.-T.; Trapp, N.; Thilgen, C.; Diederich, F.; Stöhr, M. Heat-induced formation of one-dimensional coordination polymers on Au(111): an STM study. *Chem. Commun.* **2015,** *51*, 14473-14476.
56. Campbell, C.-T.; Sprowl, L.-H.; Arnadottir, L. Reply to "Comment on 'Equilibrium constants and rate constants for adsorbates: two-dimensional (2D) ideal gas, 2D ideal lattice gas, and ideal hindered translator models'". *J. Phys. Chem. C* **2016,** *120*, 20481-20482.

FIGURES

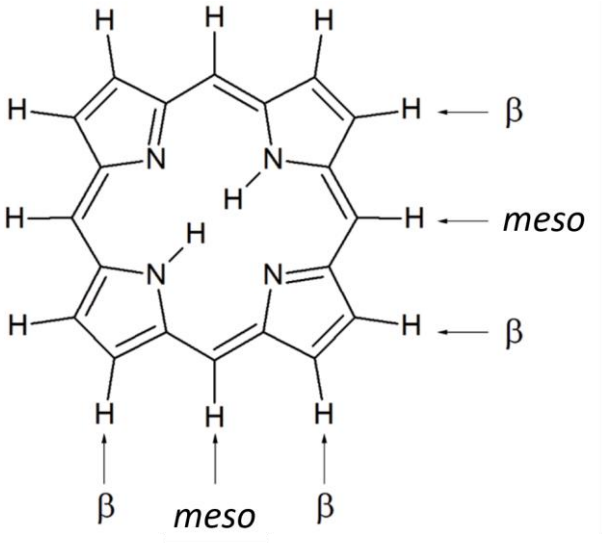

Figure 1: Chemical structure of porphine (2H-P; $C_{20}H_{14}N_4$), the parent compound of the porphyrin family. Characteristic sites for covalent linking with other molecules are located at the four pyrrole rings (β positions) and at the methine sides (meso positions) as indicated.

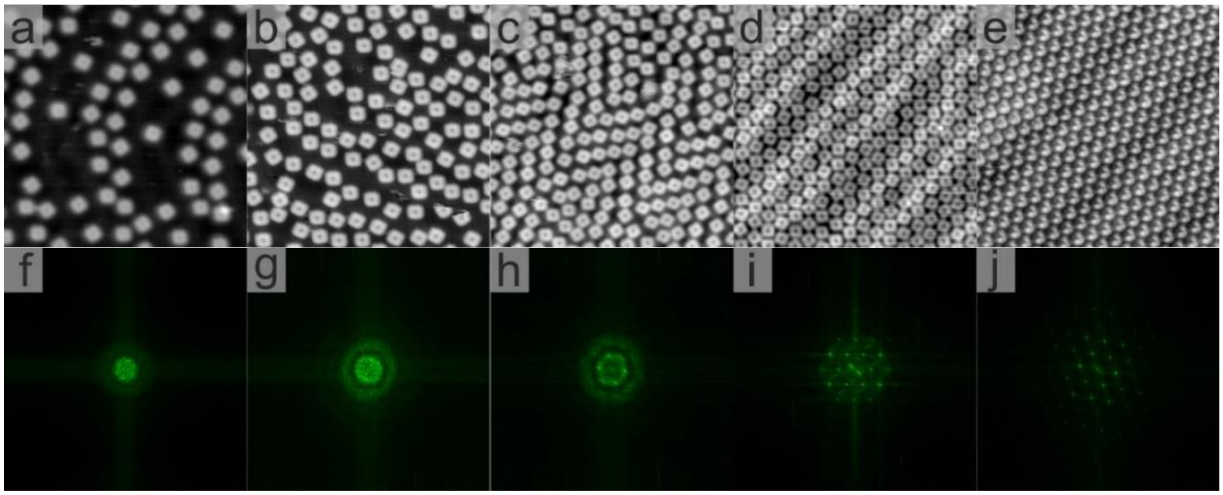

Figure 2: 2H-P molecules on Au(111) kept at room temperature during deposition. (a-e) STM images of several coverages: (a) 0.18 monolayers (ML); (b) 0.37 ML; (c) 0.49 ML; (d) 1 ML; (e) 2ML. (f-j) Fourier transformations of the images to highlight assembly symmetries. Image sizes are 18.4×18.4 nm² in (a-e) and 14×14 nm^{-2} in (f-j). The sample is kept at room temperature during deposition.

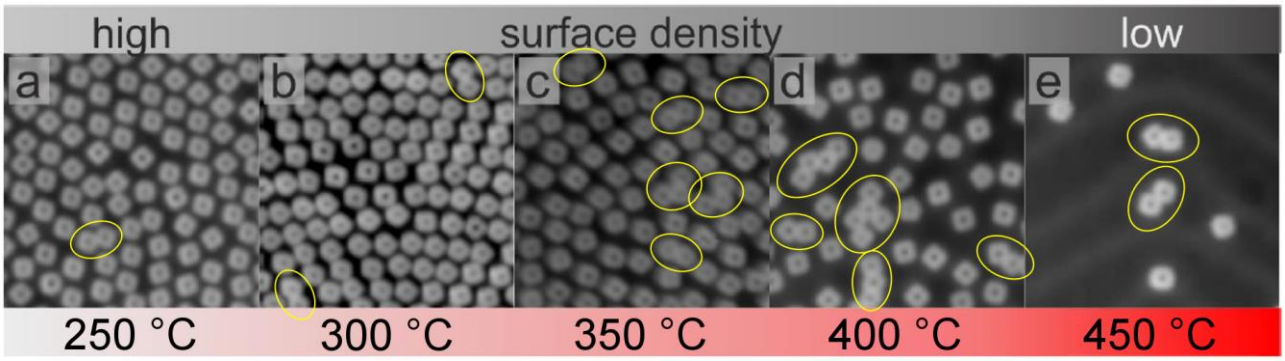

Figure 3: 2H-P molecules on Au(111) heated at different temperatures during deposition. (a-e) STM images after exposing the sample at the indicated temperatures to 180 s of porphine flux (at a rate of about 0.2 ± 0.1 ML/min).

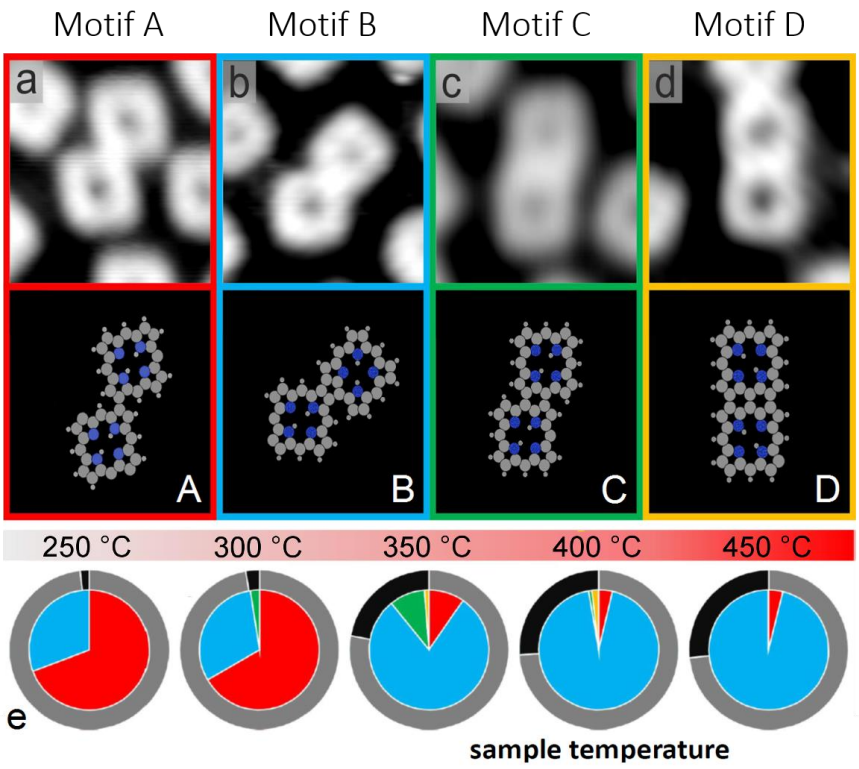

	250 °C	300 °C	350 °C	400 °C	450 °C
Motif A	69%	67%	10%	4%	4%
Motif B	31%	31%	80%	94%	96%
Motif C	0%	2%	10%	1%	0%
Motif D	0%	0%	1%	2%	0%
surf. density [mol./nm²]	0,421	0,485	0,345	0,275	0,049
reacted molecules	2%	3%	22%	26%	27%

Figure 4: Porphine dimers on Au(111). (a-d) STM topographic images of all four observed motifs with their proposed chemical structures (gas phase calculation) underneath. (a) β-β dimer with a single C-C bond (motif A), (b) (β-β), (β-meso) dimer with two C-C bonds (motif B), (c) (β-meso), (β-meso) dimer with two linkers (motif C), (d) (β-β), (meso-meso), (β-β) dimer with three connecting bonds (motif D). (e) Relative abundance for different sample temperatures during deposition with the fractions of reacted (black) and non-reacted molecules (grey) depicted on the outer ring. The complete statistics (considering both dimers and oligomers for each temperature) are given below (the dominant motif is marked in grey).

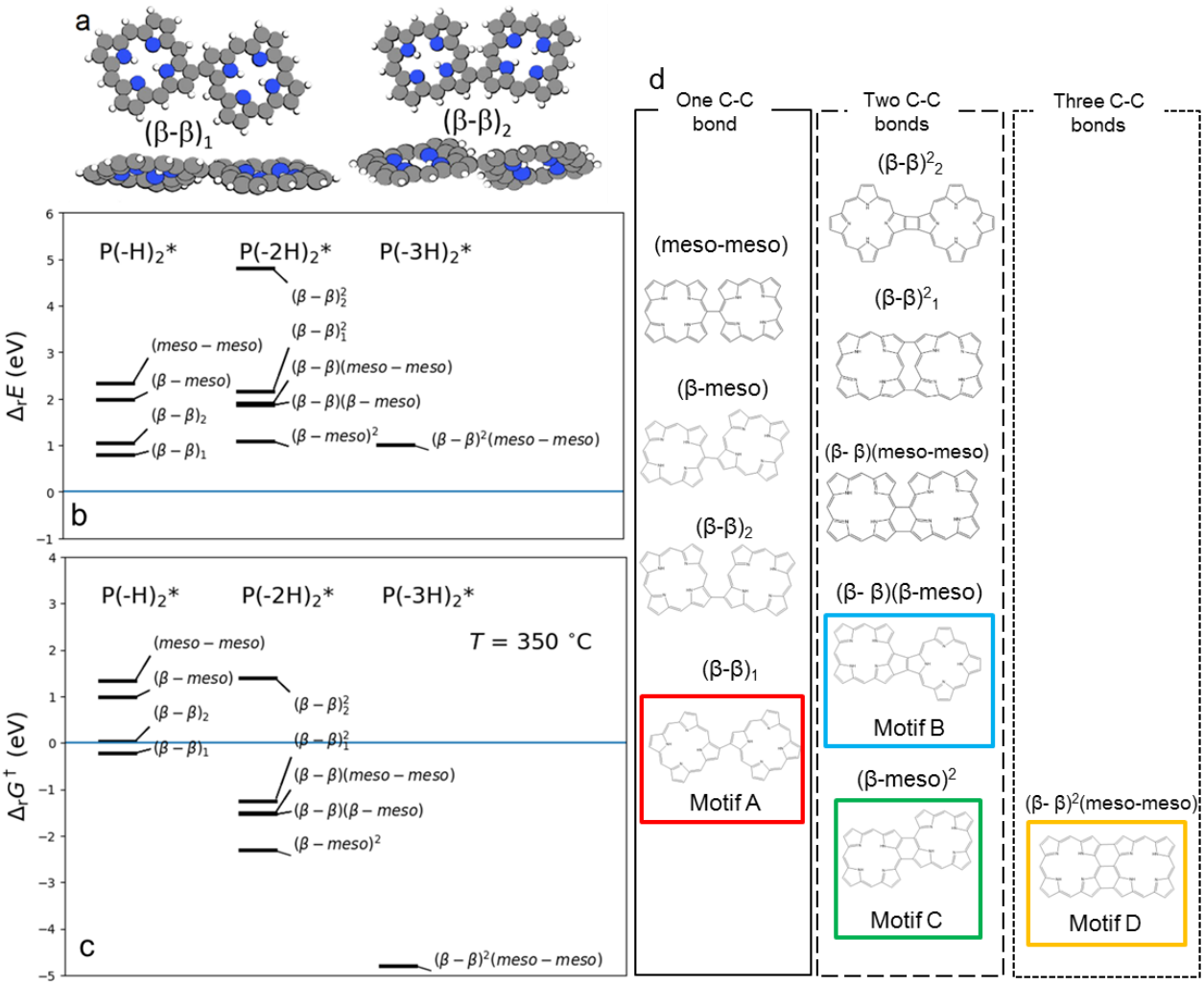

Figure 5: (a) Calculated structures of the adsorbed single-bonded $(\beta\text{-}\beta)_1$ and $(\beta\text{-}\beta)_2$ dimers, (b) reaction potential energies, Δ_rE, and (c) reaction free energies, Δ_rG, at 350 °C (note that $\Delta_rG = \Delta_rE$ at 0 K temperature) for the different dimers created with one, two or three C-C bonds. As detailed in the Supporting Information, Δ_rG was obtained at a hydrogen gas pressure of 10^{-10} mbar and using the standard-state coverage of 0.072 nm^{-2} at this temperature (see Supporting Information) as suggested by Campbell.[56] (d) Skeleton structures of each bonding motif calculated with motifs A-D highlighted in red, blue, green and yellow boxes respectively.

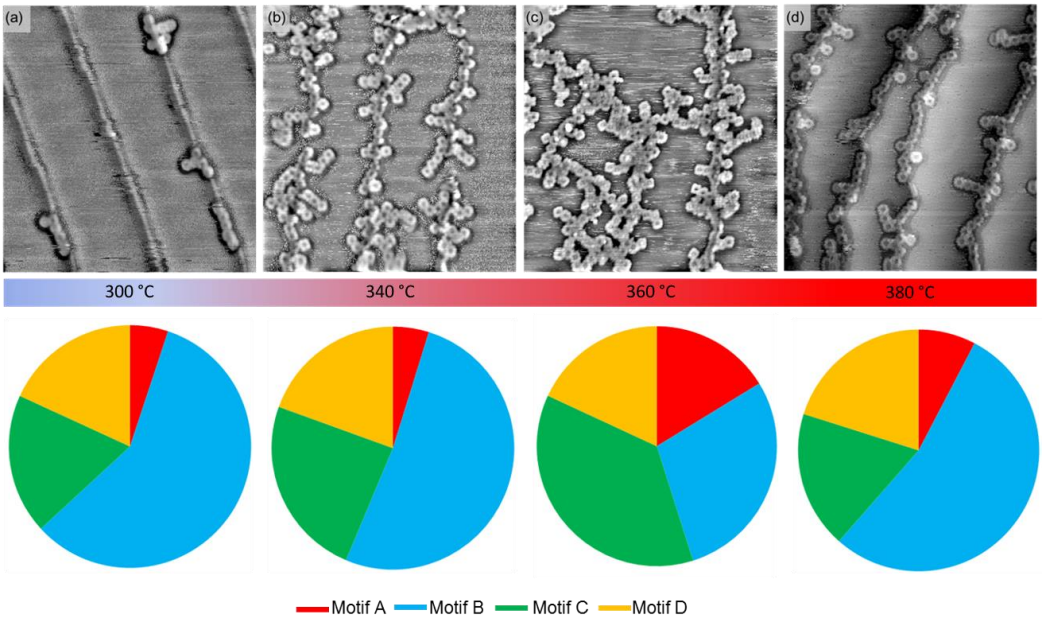

Temperature	300 °C	340 °C	360 °C	380 °C
Motif A	5%	5%	16%	8%
Motif B	58%	52%	29%	54%
Motif C	19%	24%	37%	18%
Motif D	18%	19%	18%	20%

Figure 6 : Porphine oligomers and polymers on Au(111): STM images obtained after dosing 2H-P on Au(111) at room temperature and then annealed directly to (a) 300 °C, (b) 340 °C, (c) 360 °C and (d) 380 °C (all panels are 251 nm × 265 nm in size). Images were taken at room temperature. Occurrences of different bonding motifs at step edges are shown beneath. All statistics were collected from oligomers at step edges.

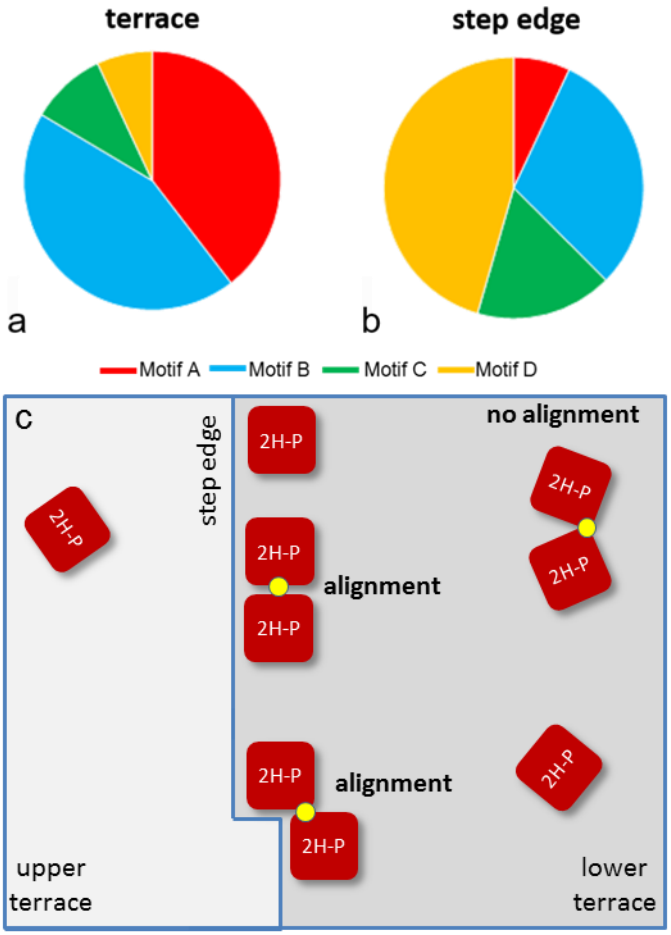

Figure 7: (a-b) Pie charts of the relative occurrence of the various binding motifs when H2-P is dosed on a Au(111) crystal held at 300 °C, obtained from STM images recorded 77K (color code: motif A – red, motif B – blue, motif C – green, motif D – yellow) on (a) terraces as compared to (b) step edges. (c) Scheme of the porphine linking process at an (idealized linear) step edge and on a terrace, with and without molecular alignment, respectively.

TABLE OF CONTENTS FIGURE